J. Opt. A: Pure Appl. Opt. **10** (2008) 125101 (13pp) doi:10.1088/1464-4258/10/12/125101

Spatial Kerr solitons in optical fibres of finite size cross section: beyond the Townes soliton

F Drouart[1], G Renversez[1], A Nicolet[1] and C Geuzaine[2]

[1] Institut Fresnel, UMR CNRS 6133, Université d'Aix-Marseille, 13397 Marseille Cedex 20, France
[2] Department of Electrical Engineering and Computer Science, Institut Montefiore B28, Université de Liège, Sart-Tilman, B-4000 Liège, Belgium

E-mail: fabien.drouart@fresnel.fr and gilles.renversez@fresnel.fr

Received 9 July 2008, accepted for publication 29 September 2008
Published 31 October 2008
Online at stacks.iop.org/JOptA/10/125101

Abstract
We propose a new and efficient numerical method to find spatial solitons in optical fibres with a nonlinear Kerr effect including microstructured ones. A nonlinear non-paraxial scalar model of the electric field in the fibre is used (nonlinear Helmholtz equation) and an iterative algorithm is proposed to obtain the nonlinear solutions using the finite element method. The field is supposed to be harmonic in time and along the direction of invariance of the fibre but inhomogeneous in the cross section. In our approach, we solve a nonlinear eigenvalue problem in which the propagation constant is the eigenvalue. Several examples dealing with step-index fibres and microstructured optical fibres with a finite size cross section are described. In each geometry, a single self-coherent nonlinear solution is obtained. This solution, which also depends on the size of the structure, is different from the Townes soliton—but converges towards it at small wavelengths.

Keywords: spatial solitons, Kerr nonlinearity, microstructured optical fibres, nonlinear optics, self-coherent solutions, Townes solitons

1. Introduction

Rigorous techniques for modelling the *linear* properties of microstructured optical fibres have been available for several years [1], and have been successfully used to study losses and chromatic dispersion of the fundamental mode [2], as well as the second mode cut-off [3]. A detailed review of these techniques with further references can be found in chapter 7 of [4].

Modelling the *nonlinear* properties of fibres (and in particular the optical Kerr effect) is inherently more complex, and while several techniques have been proposed (see e.g. [5, 6]), none is completely satisfactory. On the one hand, there are numerous works based on the nonlinear Schrödinger equation (NLSE), which do not deal with the finite size of the waveguide cross section, but focus on the transient evolution of pulse propagation along the fibre axis. The NLSE and its vector version are derived from Maxwell's equations assuming that the term $\nabla(\nabla \cdot \mathbf{E})$ in $\nabla \times \nabla \times \mathbf{E}$ can be neglected and that the slowly varying envelope approximation (SVEA) can be used [7]. On the other hand, there are (fewer) works based directly on Maxwell equations or their scalar approximation, which take into account the optogeometric profile of the fibre and do not introduce the SVEA. The NLSE and its vector version lead to a parabolic system of equations, whereas methods based directly on Maxwell's equations result in an elliptic system in the harmonic case. The differences between the two approaches have been studied extensively in [7–9]. In spite of many achievements of the NLSE (see [6]), some questions have been asked concerning its validity or its accuracy in several cases. In particular, Karlsson *et al* have shown that the use of the NLSE can give rise to wrong results for the self-phase modulation of a pulse that propagates in a bulk medium with a Kerr nonlinearity [10, 11]. Later, Ciattoni *et al* even show in [12] that several generalizations of the standard NLSE, aimed at describing non-paraxial propagation

in Kerr media, are not able to recover available exact results for TE and TM (1 + 1)-D bright spatial solitons. Only few works among the numerous articles published about spatial optical solitons deal with the genuine non-paraxial propagation of solitons. In [13], using a non-paraxial beam propagation method, the time evolution of solitons in a Kerr medium has been studied without introducing the SVEA. For several cases related either to wide angle propagation, fast varying envelope, or large spatial frequencies, it is obtained that the NLSE is not able to predict even quantitatively the time evolution given by the more accurate model based on the scalar nonlinear Helmholtz equation [13]. In [14], the time evolution of spatial solitons is computed in a (2 + 1)-D homogeneous Kerr-type nonlinear dielectric for a TM-problem using a finite-difference time-domain (FD-TD) method and the corresponding problem is solved using the NLSE. The FD-TD method shows that co-propagating in-phase spatial solitons diverge to arbitrarily large separations if the ratio of soliton beam width to wavelength is of order one or less. This is not the case for the NLSE for which the two in-phase solitons remain bounded to each other, executing a periodic separation [14]. An even more striking result was obtained by Feit and Fleck in 1988. They have shown that, for a nonlinear medium with a cubic nonlinearity, if the non-paraxiality of the beam propagation is taken into account then a finite size focusing of the optical beam is reached while with the paraxial wave equation a catastrophic collapse occurs [15].

The study presented here belongs to the second group mentioned above: it is based on the direct numerical solution of a non-paraxial scalar approximation of Maxwell's equations with non-saturable Kerr-type nonlinearities. It deals with stationary solutions and not pulse propagation. It uses the finite element method [4, 16]. We improve on previous studies in several ways. First of all, in our approach, we solve a nonlinear eigenvalue problem in which the propagation constant is an unknown of the problem; it is not fixed *a priori* or computed from the field map. Secondly, while the numerical method we propose is closely related to that proposed by Ferrando *et al* [17, 18] (we also choose a scalar nonlinear Helmholtz equation to compute the spatial solitons), we do not artificially periodize the cross section of the fibre. Its symmetry properties are thus fulfilled more easily, since no unit cell must be defined to implement the periodic boundary conditions. Thirdly, and more importantly, we do not use the 'fixed-power' algorithm proposed in [17, 18]. In this algorithm, at each step of the iterative process defined to obtain the nonlinear solution, the power of the intermediate solution is renormalized to the power arbitrarily fixed at the beginning of the algorithm [16]. Our new algorithm determines the power of the solution by itself, relying only on residue minimization. Finally, in contrast to related work by Snyder *et al* [19, 20], our algorithm can deal with inhomogeneous media [21]. As mentioned above, this is achieved by using a finite element method to solve the nonlinear problem. Although other techniques can also deal with the inhomogeneous refractive index of the fibre matrix [22], the finite element method has proved to be very efficient for the determination of propagating modes in microstructured optical fibres [23]. It is also flexible enough to represent the geometry of complex structures, and it permits a natural treatment of inhomogeneous media [21].

So as to focus on the main novel idea of our approach, only the properties of the fundamental nonlinear solutions are studied in the present paper. It is important to note that our numerical method could also deal with both high-order linear modes and higher-order nonlinear solutions.

In order to avoid any misunderstanding of the present study, we clearly state that it is not directly comparable to Bose–Einstein condensate (BEC) ones. Nonlinear optical solitons and matter–wave condensates are sometimes linked together due to the use of the NLSE (see for example [24]). Since the scalar equation we consider is different from the NLSE one, we are not allowed to take advantage of the powerful functional density method which is often used in the BEC field [25, 26]. This remark leads to at least two important consequences. The first concerns the method we have developed. It cannot be easily compared to those developed or improved for the NLSE (see section 5 of [27] and [28]) since the considered equations are different. These equations may share some general common properties but this has not been mathematically proved, at least to the best of our knowledge. Another point related to the method is that one aim of the present study is to set the basis of a non-paraxial method (solving an eigenvalue problem) in the frame of a scalar approach that can be extended to the genuine non-paraxial vector case obtained directly from Maxwell's equations. The second consequence concerns the results we obtain. We do not state that all the results obtained using our method differ from those coming from the NLSE in all cases. It is clear that when the required hypotheses are fulfilled the NLSE and our method must give similar results. But since the nonlinear scalar Helmholtz equation is nearer to Maxwell's equations than the NLSE one, the former must be considered, for stationary solutions with the $\exp(-i\beta z)$ term, as the reference one.

The paper is organized as follows. In section 2, the first steps of our self-coherent algorithm are described. The nonlinear equation derived from Maxwell's equations is defined, and the treatment of the nonlinear term and the iterative process to solve the nonlinear problem are explained. Section 3 presents how a unique self-coherent nonlinear solution can be obtained. This is explained in detail for a step-index fibre, and then more briefly for a microstructured optical fibre. In the last part of section 3, we study the convergence of the iterative process and the physical properties of the self-coherent solution obtained. A comparison with the 'fixed-power' algorithm is also performed to validate our self-coherent solution. Finally, in section 4, the physical meaning of the self-coherent solution is described. The fibre geometry dependence, including the finite size effect of the microstructured fibres, is demonstrated and a comparison with the Townes soliton [29, 30] is shown so as to prove the originality of our nonlinear solution.

2. Introduction to the new solution technique

The scalar model is considered for the propagating solution obtained under the weak guidance (weak refractive index

contrast) hypothesis [31, 32]. In this case, the electric field **E** is supposed to have only a non-vanishing transverse component of known (arbitrary) direction given by the unit vector $\hat{\mathbf{e}}$. Moreover, its divergence is usually neglected, so that $\nabla \cdot \mathbf{E} = 0$ is assumed. In the linear case, the electric field corresponding to a propagation mode is therefore a field of the form

$$\mathbf{E} = \mathfrak{Re}\left[\phi(x, y)\mathrm{e}^{-\mathrm{i}(\omega t - \beta z)}\right]\hat{\mathbf{e}} \tag{1}$$

in which $\omega = k_0 c$ is the pulsation, $k_0 = 2\pi/\lambda$ is the wavenumber and β is the propagation constant. The problem reduces to determining the function $\phi(x, y)$ and the constant β for a given value of k_0 by solving the scalar eigenvalue problem

$$\Delta_\mathrm{t}\phi + k_0^2\varepsilon_\mathrm{r}\phi = \beta^2\phi, \tag{2}$$

where Δ_t is the transverse Laplacian. This equation is obtained from Maxwell's equations with materials of relative permittivity ε_r and using all the hypotheses above. The dispersion curves are the set of pairs (k_0, β) for which a solution of equation (2) exists.

The relative permittivity is itself a function of the field intensity and the following dependence is assumed:

$$\varepsilon_\mathrm{r}(\phi) = n_0^2 + \mathbb{I}_\mathrm{nl} n_\mathrm{Kerr}^2 |\phi|^2 \tag{3}$$

in which $\mathbb{I}_\mathrm{nl}$ is the indicative function equal to one in the nonlinear case (where the fibre is made of an optical Kerr material) and zero elsewhere, and where n_0 (the linear refractive index) and $n_\mathrm{Kerr}^2 = 3\chi^{(3)}/2\epsilon_0 c n_0$ (the Kerr coefficient) are constants characterizing the material [17, 33].

As the nonlinearities depend only on the modulus of the field and not on its instantaneous value, it may be possible to obtain solutions that can be represented by equation (1). This is our fundamental hypothesis. We are therefore looking for solutions (β, ϕ) of the nonlinear equation

$$\Delta_\mathrm{t}\phi + k_0^2(n_0^2 + \mathbb{I}_\mathrm{nl} n_\mathrm{Kerr}^2 |\phi|^2)\phi = \beta^2\phi. \tag{4}$$

When a single Kerr material is used, setting the reduced field

$$\phi_\mathrm{r} = n_\mathrm{Kerr}\phi \tag{5}$$

allows one to reduce equation (4) to

$$\Delta_\mathrm{t}\phi_\mathrm{r} + k_0^2(n_0^2 + \mathbb{I}_\mathrm{nl}|\phi_\mathrm{r}|^2)\phi_\mathrm{r} = \beta^2\phi_\mathrm{r}, \tag{6}$$

which is independent of the Kerr coefficient. Clearly, this means that the refractive index profile leading to the self-coherent solution ϕ_r depends on the linear part of the medium but not on the value of the Kerr coefficient n_Kerr: only the quadratic dependence matters. The physical field $\phi = \phi_\mathrm{r}/n_\mathrm{Kerr}$, however, depends on the coefficient n_Kerr: the smaller n_Kerr, the larger the power injected to produce the self-coherent solution.

We use a finite element method [4] to solve equation (4). As mentioned in section 1, this method is well adapted. This is not the case of the well-known multipole method [1] for which the refractive index of the matrix surrounding the inclusion must be homogeneous. The more recent fast Fourier factorization mode searching method is able to deal with an inhomogeneous medium [22]. Nevertheless, like the multipole method, it has been directly developed in the vector case not in the scalar one. Furthermore, since one of the final goals of our work is to solve the full vector nonlinear problem, it is more convenient for us to use the finite element method for which we already have both the scalar and the vector formulations of the linear problem.

In the present case of a scalar model, we use a classical finite element approximation based on piecewise linear interpolation on a triangular mesh. Moreover, the solutions are supposed to be close to the modes of the linear fibre and therefore the proposed algorithm is a simple Picard iteration, in which a propagation mode is computed in a linear fibre with a refractive index profile determined by the field intensity obtained at the previous iteration.

The starting point of our algorithm is thus the linear fibre; i.e., no nonlinear Kerr effect is considered. For a given k_0, some modes are computed (by solving a matrix eigenvalue problem to find the βs and the corresponding electric fields) and the mode of interest is selected (e.g., the fundamental mode). The corresponding electric field (whose amplitude is arbitrarily fixed in the linear fibre only) is used to compute the new refractive index profile, then new modes are computed with this given refractive index. The mode of interest is selected and used to modify again the refractive index profile that gives a new eigenvalue problem. This process is repeated until the refractive index profile and the β value reaches a fixed point.

This process seems quite simple but there is a fundamental flaw: the amplitude of the eigenmodes is irrelevant and the numerical solutions of the intermediary eigenvalue problems have an uncontrolled amplitude. To the contrary, the nonlinear problem depends fundamentally on the amplitude of the field, and therefore this amplitude has to be determined *a posteriori* for the mode of interest. The chosen solution $\psi(x, y)$ of the numerical eigenvalue problem has thus to be scaled by a scalar factor χ to obtain the reduced field

$$\phi_\mathrm{r} = \chi\psi \tag{7}$$

which corresponds to normalizing the field ψ. A suitable numerical value of χ may be obtained by cancelling a weighted residual of equation (6), with the solution ψ itself taken as the weight factor (so as to minimize the error where the field has the largest values).

In detail, here is how this normalization procedure is applied. First, (ψ_i, β_i) at step i $(i \geqslant 1)$ are computed as particular solutions to the eigenvalue problem

$$\Delta_\mathrm{t}\psi_i + k_0^2(n_0^2 + \mathbb{I}_\mathrm{nl}|\phi_{r,i-1}|^2)\psi_i - \beta_i^2\psi_i = 0, \tag{8}$$

in which, at $i = 1$, $\phi_{r,0}$ is the solution of the linear problem. Then, the value of χ_i is computed so as to optimize the self-coherence of $\phi_{r,i} = \chi_i\psi_i$ by cancelling the residue

$$\int_K \left[\Delta_\mathrm{t}\psi_i + k_0^2(n_0^2 + |\chi_i\psi_i|^2)\psi_i - \beta_i^2\psi_i\right]\overline{\psi_i}\,\mathrm{d}S = 0, \tag{9}$$

where the integral is computed on the cross section K of the Kerr medium region ($\overline{\psi_i}$ represents the complex conjugate of

ψ_i). Using this equation as is would lead to an ill-conditioned expression for χ_i, due to the subtraction of two terms of very similar magnitude. Using the following identity derived from equation (8),

$$\int_K \left[(\Delta_t\psi_i + k_0^2 n_0^2 \psi_i - \beta_i^2\psi_i)\overline{\psi_i}\right] \mathrm{d}S = \int_K k_0^2 |\phi_{r,i-1}|^2 \psi_i \overline{\psi_i}\, \mathrm{d}S, \tag{10}$$

a numerically well-conditioned expression for χ_i can be obtained:

$$\chi_i^2 = \frac{\int_K |\psi_i|^2 |\phi_{r,i-1}|^2 \,\mathrm{d}S}{\int_K |\psi_i|^4 \,\mathrm{d}S}. \tag{11}$$

The whole procedure is summarized in the following algorithm [16]:

begin:

- Set $\psi_0 = 0$ (linear case), $\chi_0 = 1$, $i = 1$
- **repeat**
  - Compute the eigenfunctions ψ_i and the corresponding β_i via the finite element solution of the eigenvalue problem defined by equation (8) and select the one of interest (e.g., the fundamental).
  - Compute χ_i via formula (11).
  - Set $i \leftarrow i + 1$.
- **until** the absolute value of the relative difference between β_i and β_{i-1} denoted by $\delta_i^{\mathrm{relat}}$ is smaller than a prescribed tolerance.
- The $(\chi_{\mathrm{coh}}\psi_{\mathrm{coh}}/n_{\mathrm{Kerr}} = \phi_{\mathrm{coh}}, \beta_{\mathrm{coh}})$ of the last iteration is the self-coherent solution.

end.

Therefore, the proposed algorithm allows us to find a self-coherent solution from an initial solution of the linear problem normalized at one ($\chi_0 = 1$). We call this algorithm the SC_{LinN} algorithm. This process renormalizes the field at each iteration and we can thus deduce the 'self-coherent' power *a posteriori*: it is defined as the integral of $\chi_{\mathrm{coh}}^2\psi_{\mathrm{coh}}^2$.

3. Towards a unique self-coherent solution

Numerical experiments show that the SC_{LinN} algorithm seems sensitive to the amplitude and the shape of the initial field used to start the iteration. To study this feature, a scan of the amplitude and of the shape of the initial solution is performed. To evaluate quantitatively the quality of a solution obtained at the convergence according to the starting point, we propose a criterion: the residue given by the left-hand side of equation (9) is calculated numerically with the finite element approximation of ψ_i.

The numerical tests concern two types of fibre: step-index fibres and microstructured optical fibres. Moreover, we are only interested in the fundamental mode in the linear case. The nonlinear solution associated with this fundamental mode will be referred to as the *nonlinear fundamental 'mode'*. We put 'mode' in between quotation marks, as it is not a mode such as defined in the linear case—there is no superposition principle. Our finite element code has been validated for the computation of modes in linear microstructured fibres, by comparing the results with the well-established multipole method [1, 2] and with the more recent fast Fourier factorization mode searching method which is more versatile [22].

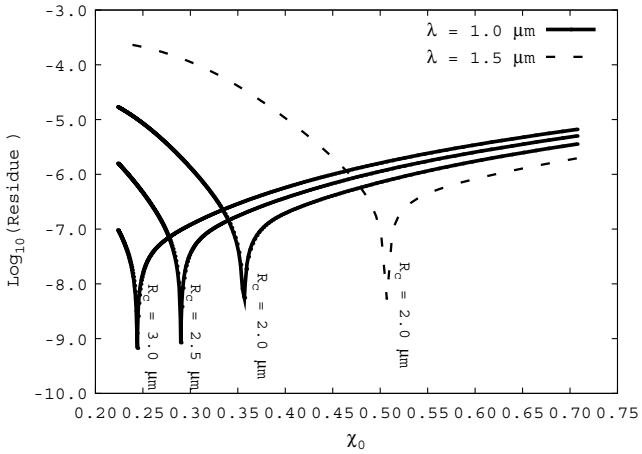

Figure 1. Logarithm of the residue obtained at the convergence, computed using the left-hand side of equation (9), versus the field amplitude χ_0 for two different wavelengths and three different core radii of the step-index fibre.

To correctly describe the field in the fibre and to minimize the computation time, an adaptive mesh refinement is used: the stronger the field, the finer the mesh. In addition, the convergence of the SC_{LinN} algorithm has been shown in [16], and in all the following tests we choose the prescribed tolerance $\delta_i^{\mathrm{relat}} < 10^{-10}$.

3.1. Scanning the amplitude of the linear initial field for the step-index fibre

We start by studying the influence of the amplitude χ_0 of the initial (linear) field $\phi_{r,0}$. For this, we inject $\chi_0\psi_0$ at the first iteration in the nonlinear term in equation (8):

$$\Delta_t\psi_1 + k_0^2(n_0^2 + \mathbb{I}_{\mathrm{nl}}|\chi_0\psi_0|^2)\psi_1 - \beta_1^2\psi_1 = 0, \tag{12}$$

in which the amplitude χ_0 is arbitrarily fixed. Therefore, the initialization of the SC_{LinN} by a unique initial guess is replaced by a one-dimensional scan of the amplitude of the linear initial solution. We denote this process the SC_{Lin1D} algorithm.

In addition, to start the study of SC_{Lin1D}, a cylindrical fibre with a Kerr material ($n_{\mathrm{Kerr}} = 3.2 \times 10^{-20}$ m^2 W^{-1}) in the circular core of radius 2.0 μm is considered. The linear part of the refractive index of this core is $n_0 = 1.45$. The core is embedded in an infinite cladding with a linear refractive index $n = 1.435$ (weak guidance approximation WGA). The Dirichlet condition at the edge of the geometry is also applied (in the present paper we do not address the computation of the leaky modes [1, 4]).

Figure 1 gives the effect of the initial field amplitude on the residual values defined by the left-hand side of equation (9), for different wavelengths and geometries.

Figure 1 shows the minimum residue for the nonlinear solution at the convergence of the iterative process (i.e. when $\delta_i^{\mathrm{relat}} < 10^{-10}$, the fixed point is reached). The influence of

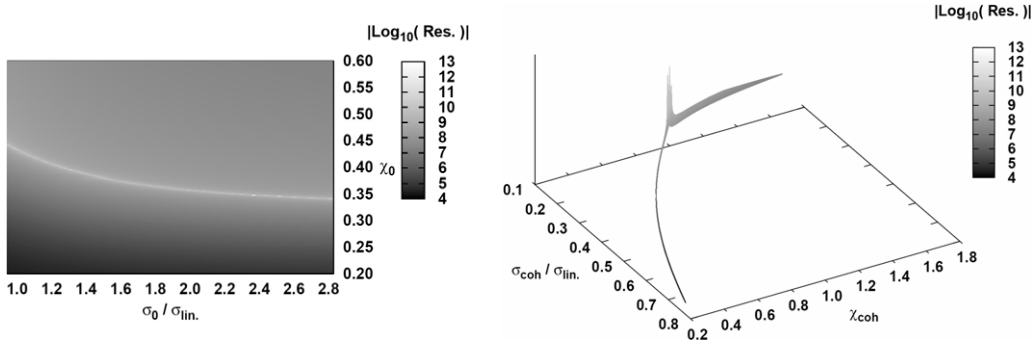

(a) Final residue versus initial parameters χ_0 and $\sigma_0/\sigma_{lin.}$

(b) Final residue versus final parameters χ_{coh} and $\sigma_{coh}/\sigma_{lin.}$ (see the text for a complete description)

Figure 2. Maps of the residue computed for the nonlinear solution as a function of the input parameters characterizing the initial field (a) and as a function of the output parameters characterizing the nonlinear field (b) of the step-index fibre described in the text at $\lambda = 1.0\ \mu$m. σ_{lin} corresponds to the standard deviation of the solution of the linear problem approximated by a Gaussian function.

the mesh has been ruled out by verifying that the minimum corresponds to the same χ_0 for different meshes. It may be deduced that a single nonlinear solution is found for each wavelength: it is *the self-coherent nonlinear solution*. Obviously there exists another minimum residue for $\chi_0 = 0$, corresponding to the solution of the linear problem.

3.2. Scanning both the amplitude and the width of the initial field

In a further investigation, the residue is considered by scanning the initial solution not only in amplitude but also in shape. At the first iteration, instead of the solution of the linear problem, we inject a Gaussian function $\chi_0 e^{-(r/\sigma_0)^2}$, where $r = \sqrt{x^2 + y^2}$ and where σ_0 represents the standard deviation of the function. Therefore, the initialization of the SC_{Lin1D} algorithm is replaced by a two-dimensional scan on χ_0 and σ_0. We call this process the $SC_{Gauss2D}$ algorithm.

The computation is started with one value of σ_0 and the scan in χ_0 is performed, then another value of σ_0 is taken, and so on. Finally, the residue at the convergence of $SC_{Gauss2D}$ is obtained, according to the two parameters χ_0 and σ_0 characterizing the initial field, as shown in figure 2(a).

A narrow valley of minimal residues is observed. This means that for one σ_0 there exists a single χ_0 such that one 'good' final nonlinear solution is obtained: it is the self-coherent solution. Notice that the linear case corresponds to a vertical line in the figure 2(a) at $\sigma_0/\sigma_{\text{lin}} = 1$ when the Gaussian profile closely matches the profile of the fundamental mode as in the WGA. Figure 2(a) suggests that there exists a continuum of solutions depending on the value of σ_0 given for each minimum of the residue. Thus, the question is whether the nonlinear solutions obtained with the solution of the linear problem or each Gaussian function (characterized by σ_0) as the starting point are the same: is the self-coherent solution really unique?

Figure 2(b) shows the absolute value of the logarithm of the residue according to the final solution parameters $(\chi_{\text{coh}}, \sigma_{\text{coh}})$, in which we approximate this nonlinear solution with a Gaussian fit. This figure shows that these final parameters have nearly the same value. Therefore, from a full map of the initial parameters, the $SC_{Gauss2D}$ algorithm provides a localized surface formed by the final parameters characterizing the computed nonlinear solution. In addition, the minimum residues are localized in a small part of this surface. These results allow us to confirm the assumption that the $SC_{Gauss2D}$ algorithm finds a single nonlinear solution: the self-coherent nonlinear solution. This solution is a scalar spatial Kerr soliton in the step-index fibre.

Since for both studied cases (SC_{Lin1D} and $SC_{Gauss2D}$ algorithms) only a unique residue minimum associated to a nonlinear solution (corresponding to the same β value) is found for all the step-index fibres and wavelengths we have tested, we can assume that this observed rule is general for this kind of fibres.

3.3. Results for the microstructured optical fibre

Microstructured optical fibres (MOFs) have more degrees of freedom related to the geometries and index contrasts than step-index fibres [4]. The study of these fibres allows us to extend the domain of validity of our algorithm and to compare our results with those previously published in [17]. The case of a solid core MOF made of four rings of air holes embedded in a Kerr material matrix ($n_{\text{Kerr}} = 3.2 \times 10^{-20}$ m^2 W^{-1}) is considered here. The linear part of the refractive index in the matrix is $n_0 = 1.45$. The pitch Λ (space between the centre of two adjacent air hole centres) is equal to 10.0 μm and the air hole radius is equal to 2.75 μm.

As for the step-index fibre, the results obtained with SC_{Lin1D} show two minima for the residue: one associated with the solution of the linear problem ($\chi_0 = 0$) and one corresponding to the nonlinear solution. Whatever the amplitude of the solution of the linear problem, a single nonlinear solution—the self-coherent solution—is again found.

For the $SC_{Gauss2D}$ algorithm the Gaussian function is injected only in the matrix and not in air holes since the

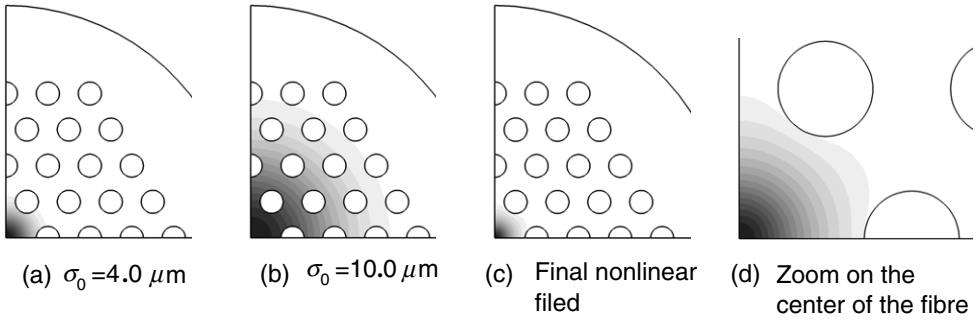

Figure 3. Field distribution in the microstructured optical fibre at $\lambda = 5.0$ μm for two initial Gaussian fields ((a) and (b)) and for the fundamental soliton ((c) and (d)).

field is usually very weak in the air holes due to the index contrast between the matrix and the inclusions. As for the step-index fibre, there is a narrow valley (similar to that of figure 2(a)) corresponding to the minimal values of the residue as a function of the initial parameters χ_0 and $\sigma_0/\sigma_{\text{lin}}$. The map of the final residue versus the final parameters χ_{coh} and $\sigma_{\text{coh}}/\sigma_{\text{lin}}$ obtained is similar to that of figure 2(b).

Figure 3 shows the field distribution when the Gaussian function is used as an initial field, as well as the effect of the nonlinearity when $SC_{Gauss2D}$ has converged. (Using the symmetry properties of the fibre, only a quarter of the geometry needs to be modelled, which significantly reduces the cost of the numerical computations.) These figures illustrate the independence of the final self-coherent nonlinear solution according to the spatial extent of the input initial field.

Therefore both for step-index fibres and for MOFs, SC_{Lin1D} and $SC_{Gauss2D}$ lead to the same solution: the self-coherent solution. Actually, the most natural choice for the physical studies is to use SC_{Lin1D} in which the starting point depends on the solution of the linear problem.

Note that a very fine scan must be performed to obtain the minimum value of the residue equal to the machine accuracy (10^{-15}). Consequently, in practice, the speed and accuracy of the algorithm SC_{Lin1D} are improved by using the golden section search in one dimension [34]. For each wavelength studied, the search is performed on the value of χ_0. The typical shape of the function to be minimized is that in figure 1. Using this improvement, the algorithm is able to reach machine accuracy for the minimal values of the computed residues.

3.4. Physical significance of the self-coherent solution: comparison with the 'fixed-power' method

A 'fixed-power' method was proposed by Ferrando *et al* in [17, 18] to find nonlinear solutions in MOFs with a Kerr term in the matrix refractive index. We call this process, in which the power is given *a priori*, the algorithm FP_{Fer}. Our algorithm SC_{LinN} can be easily modified (to study the 'fixed-power' method) by replacing equation (11) with $\chi_i^2 = P/\int_K |\psi_i|^2 \, \mathrm{d}S$, in which P is the fixed value of the power. We call our finite element method implementation of the 'fixed-power' process the FP_{FEM} algorithm.

To compare the physical properties of the solutions given by FP_{Fer}, FP_{FEM}, and SC_{Lin1D}, we use the quantities

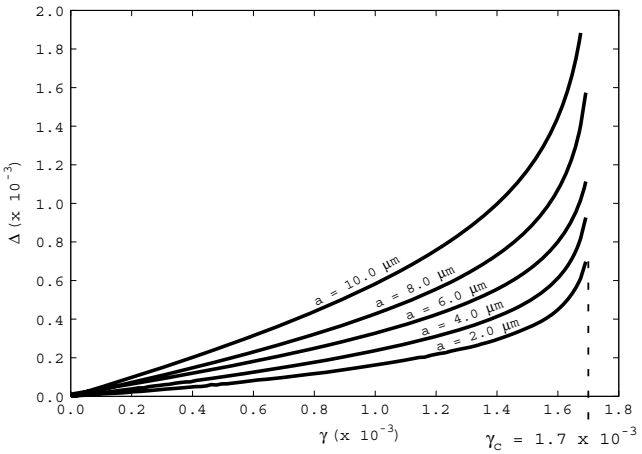

Figure 4. Dependence of the gap function Δ on the nonlinear coefficient γ for various air hole radii a at $\lambda = 1.55$ μm. These results are obtained by using the algorithm FP_{FEM}, and γ_c is defined in the text.

defined in [17]: the dimensionless nonlinear coefficient $\gamma = Pn_{\text{Kerr}}^2/A_0$ and the gap function $\Delta = (\beta_{\text{NL}} - \beta_{\text{lin}})/k_0$, in which P is the total power, and $A_0 = \pi(\Lambda/2)^2$ characterizes the core size (for the step-index fibre, $A_0 = \pi R_{\text{core}}^2$, in which R_{core} is the radius of the core). β_{lin} and β_{NL} are the propagation constants of the solution of the linear and nonlinear problems, respectively.

Our first study consists in comparing the results of the two implementations of the 'fixed-power' method: FP_{Fer} and FP_{FEM}. The computations are provided for a silica microstructured optical fibre with a pitch equal to 23.0 μm, for various air hole radii at $\lambda = 1.55$ μm [17]. The MOF considered in FP_{FEM} has a finite size and is made of four rings of air holes, while the geometry for FP_{Fer} is periodic. The evolution of the gap function Δ according to the nonlinear coefficient γ is computed (see figure 4) for various air hole radii. This figure shows an approximate limit power corresponding to $\gamma_c = 1.7 \times 10^{-3}$. As soon as $\gamma > \gamma_c$ the numerical process is divergent. Figure 4 shows that the value of γ_c found with FP_{FEM} is the same as that obtained with FP_{FEM} (see figure 3(a) in [17]).

The second study consists in understanding the physical significance of the self-coherent solution. To achieve this,

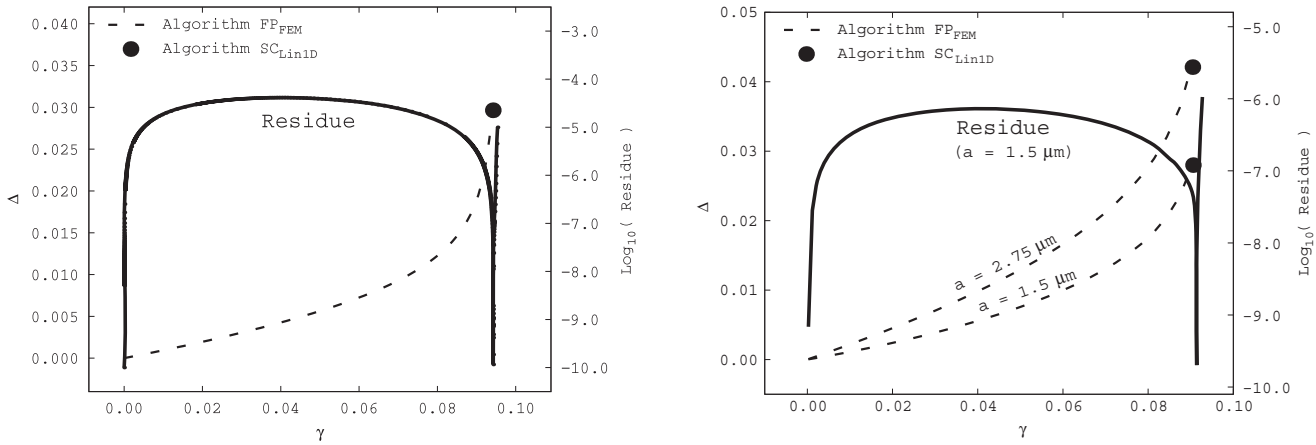

(a) Comparison for the step-index fibre described in section 3.1 at λ = 1.0 μm and the corresponding residue

(b) Comparison for two MOFs with different radii *a* at λ = 5.0 μm and one associated residue for *a* =1.5 μm

Figure 5. Comparison between FP_{FEM} and SC_{Lin1D} for the fundamental 'mode' for different fibres. γ_c corresponds to the critical power; above this value FP_{FEM} diverges.

the physical powers obtained by FP_{FEM} and SC_{Lin1D} are compared. Therefore, this study consists in getting the value of the 'self-coherent power' (i.e., $P_{coh} = \int_F |\chi_{coh}|^2 |\psi_{coh}|^2 \, dS$) obtained using SC_{Lin1D}. Then, the value of the physical power equal to $P_{phys.} = P_{coh}/n_{Kerr}^2$ is deduced. Finally, some ascending values of power are injected as input in FP_{FEM} until the value of the physical power $P_{phys.}$ obtained with SC_{Lin1D} is reached. Figure 5 gives the results of this comparison for several fibres: the step-index one, figure 5(a), and two microstructured optical ones with different air hole sizes, figure 5(b).

Figure 5(a) shows the comparison between FP_{FEM} and SC_{Lin1D} for the step-index fibre described in section 3.1 at $\lambda = 1.0$ μm. The 'fixed-power' algorithm FP_{FEM} diverges for power γ above the critical power γ_c (see figure 4). Contrary to the results provided by FP_{Fer} in [17], the critical γ computed with FP_{FEM} depends slightly on the air hole radius a. As will be shown in the next paragraph, this dependence is confirmed using SC_{Lin1D}. This issue is also discussed in section 4.

The self-coherent algorithm SC_{Lin1D} finds the self-coherent solution at the corresponding critical power directly. As mentioned at the end of section 3.1, two minimal values of the residue are found. The first one corresponds to the linear case $\gamma = 0$ and the second one corresponds to the self-coherent nonlinear solution. This solution is obtained both with SC_{Lin1D} and with $SC_{Gauss2D}$. The other solutions found with the 'fixed-power' method at lower powers are not the self-coherent solution because they do not correspond to a minimal residue.

To complete this observation, the study is repeated for various MOFs (figure 5(b)). The computed results for these two MOF geometries lead to the same conclusion as that already drawn for the step-index fibre: the self-coherent solution obtained with the algorithm SC_{Lin1D} gives directly (and so, much more rapidly) the limit of the highest power solution reachable ($\gamma = \gamma_c$) with the algorithm FP_{FEM}.

Therefore, with our new SC_{Lin1D} algorithm and for each fibre, a single self-coherent solution corresponding to the spatial soliton with the highest possible energy just before the self-focusing instability is easily obtained.

The last study is to compare the convergence of SC_{Lin1D} with the one of the 'fixed-power' method FP_{FEM} (figure 6).

This figure shows the comparison of the convergence for two different powers (represented by the γ coefficient) in the MOF described in section 3.3. Figure 6 proves that SC_{Lin1D} converges much more rapidly than FP_{FEM}. After 50 steps the convergence of FP_{FEM} is not reached, whereas SC_{Lin1D} requires 13 steps to converge. In addition, at the critical power ($\gamma = \gamma_c$), that is to say for the self-coherent solution, the effective index cannot be found with FP_{FEM} because this algorithm does not reach the required accuracy (for $\delta_i^{relat} < 10^{-10}$) unlike the self-coherent algorithm SC_{Lin1D}.

4. Beyond the Townes soliton

As illustrated in figure 5, the self-coherent solution corresponds to the spatial soliton with the highest reachable power before the self-focusing instability. Therefore, we can wonder whether this solution is the solution obtained for a homogeneous silica medium with a nonlinear Kerr term [29]. To analyse this issue, SC_{Lin1D} is implemented for this case and the results are compared with those given by the following fibre geometries (figure 7): the step-index fibres with various core radii in the case of the WGA described in section 3.1, and different solid core microstructured optical fibres with various air hole radii.

Figure 7 shows that the self-coherent solution of the nonlinear step-index fibre depends on the core radius. This means that, even in the nonlinear case, the core/cladding interface is important. The curves given in figure 7 also prove that the nonlinear solution obtained in the step-index fibres differs from that of the homogeneous medium. As

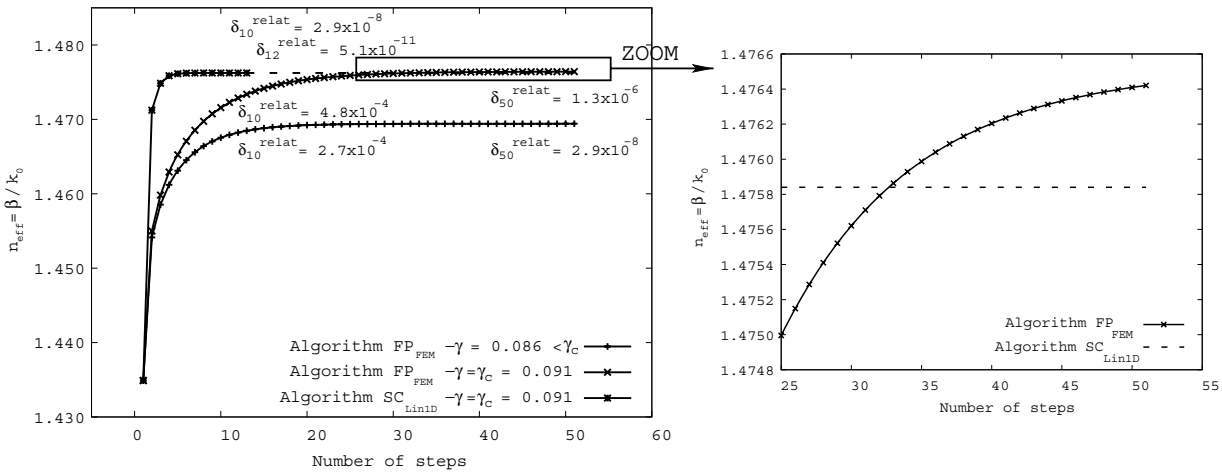

Figure 6. Convergence of SC_{Lin1D} compared with FP_{FEM} for the fundamental 'mode' of the MOF described in section 3.3 at $\lambda = 5.0\ \mu$m. δ_i^{relat} is the absolute value of the relative difference between the values of β at the steps $i-1$ and i. To make the comparison with the FP_{FEM} results easier, the value of n_{eff} for the self-coherent solution at step 13 of the SC_{Lin1D} is extended to step 50.

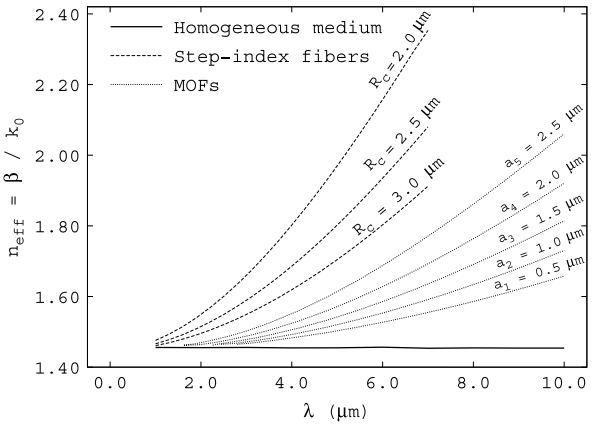

Figure 7. Comparison of the nonlinear effective index of the spatial soliton versus the wavelength in different nonlinear waveguides and in a homogeneous nonlinear medium. The solid core MOFs studied have four rings of air holes with various radii a and $\Lambda = 6.0\ \mu$m. The index contrast of the step-index fibres with various core radii fulfils the WGA.

expected, the higher the core radius (i.e. the structure tends to the homogeneous medium), the smaller the difference with the homogeneous medium. The same phenomenon is observed for the MOFs, where the self-coherent solution does not correspond to that obtained in the homogeneous medium. In addition, the smaller the air hole radius (i.e. the structure tends to the homogeneous medium), the smaller the difference with the homogeneous case. Figure 7 also shows that for smaller wavelengths the role of the air holes decreases, the self-coherent solution being more confined. Notice that, in the 'fixed-power' study [17], the ratio λ/Λ is small. This explains the weak influence of the fibre geometry on the critical nonlinear coefficient γ_c. As a consequence, the diagram of existence of spatial solitons (figure 3(b) in [17]) must be modified so as to take into account the influence of the waveguide geometry. In the parameter space (γ, a) and using the terminology defined in [17], the frontier between the *spatial soliton* region and the *self-focusing* region is not exactly a vertical line defined by a unique critical nonlinear coefficient γ_c. It is rather a line segment such that the lower the nonlinear coefficient the bigger the hole radius. The limit case corresponds to a step-index fibre with nonlinear core surrounded by an air ring with the hole diameter $d = 2a = \Lambda/2$ (see figure 7).

Therefore, the spatial solitons obtained with our algorithm for nonlinear optical waveguides differ from that of a nonlinear homogeneous medium.

The second point concerns the study of the Townes soliton [17, 29, 30]. The Townes soliton corresponds to the solution of a propagation problem in a nonlinear homogeneous medium. It corresponds to the critical solution before the self-focusing instability. We recall that the genuine Townes soliton, as defined in the seminal article written by Chiao *et al*, is obtained without using the SVEA (see equations (5) and (6) in [29]) but the propagation constant of the soliton is computed from the field profile. The problem solved (see the paragraph below equation (6) in [29]) is not an eigenvalue problem. To assert the difference between our self-coherent solution obtained for each structure with the Townes soliton, the power and the profiles of these solutions are studied. The first step is to get the profile $R(r)$ of the Townes soliton as the solution of the one-dimensional (1D) equation:

$$\Delta_t R - R + R^3 = 0, \qquad R'(0) = 0 \qquad \text{and} \qquad R(\infty) = 0. \tag{13}$$

To solve this two-point boundary value problem a shooting method is used [34]. The profile of the solution is obtained and shown in figure 1 of [29]. We have also calculated the critical power coefficient N_{cr} [30] given by

$$N_{\text{cr}} = \int_{\Omega} |R|^2 r\, \mathrm{d}r \approx 1.862 \tag{14}$$

where Ω corresponds to the 1D domain.

To compare our self-coherent solution with the Townes one, an expression of the self-coherent power N_{coh} associated

with the critical power coefficient N_{cr} is defined. In physical units, the lower bound of the critical power P_{cr}^{lb} is given by [30, 33]

$$N_{cr} = \frac{4\pi n_0 n_2}{\lambda^2} P_{cr}^{lb} \tag{15}$$

where n_2 represents the nonlinear coefficient characterizing the Kerr medium. The scalar optical Kerr effect can be defined as follows: $\varepsilon_r(\phi) = (n_0 + n_2|\phi|^2)^2 \approx n_0^2 + 2n_0 n_2|\phi|^2$, and we have defined $n_{Kerr}^2 = 2n_0 n_2$, in which n_2 is the nonlinear coefficient characterizing the material [5]. However, in our case, an eigenvalue-like problem is solved. Indeed, unlike the Townes soliton studies [29, 30], the propagation constant β is considered so as to describe completely the features of the nonlinear self-coherent solution. To take into account the β_{coh} eigenvalue of our approach, the physical power P_{phys} defined directly from the Poynting theorem is calculated. In this case,

$$P_{phys} = \frac{\beta_{coh}}{\tilde{k}_0} P_{cr}^{lb} = \frac{P_{coh}}{n_{Kerr}^2} = \frac{P_{coh}}{2n_0 n_2}, \tag{16}$$

in which $P_{coh} = \int_\Omega |\chi_{coh}|^2 |\psi_{coh}|^2 \, dS$ is the self-coherent power obtained at the convergence of SC_{Lin1D}, and $\tilde{k}_0 = 2\pi n_0/\lambda$ is defined so as to compare with the critical power coefficient N_{cr} given in [30]. Consequently, we get

$$P_{cr}^{lb} = \frac{\tilde{k}_0}{2n_0 n_2 \beta_{coh}} P_{coh}. \tag{17}$$

Therefore, the coefficient N_{coh} permitting us to compare our scalar spatial Kerr solitons with the Townes soliton can be defined, by using P_{cr}^{lb} of the equation (17) in expression (15), as

$$N_{coh} = \frac{4\pi^2 n_0}{\beta_{coh}\lambda^3} P_{coh}. \tag{18}$$

Figure 8 shows the comparison between the coefficient N_{coh} for step-index fibres with various core radii, for solid core MOFs with various air hole sizes, and for the homogeneous medium with the critical power coefficient N_{cr} of the Townes soliton. These results confirm those obtained in figure 7, and they illustrate the influence of the fibre geometry. In addition, figure 8 shows that the smaller the wavelength (the field is more confined in the MOF core), the smaller the difference between the Townes soliton and the self-coherent solutions.

Figure 8 also gives the evolution of the value of N_{coh} in the homogeneous medium case, with respect to the wavelength. As explained above, our numerical approach SC_{Lin1D} takes into account the β value. Nevertheless, it is very near the constant one of the genuine Townes soliton (1.4555 instead of 1.45). A more detailed wavelength dependence cannot be obtained with the current numerical accuracy of the effective indices. We can recall that it is known from the seminal work of Chiao *et al* that for the Townes soliton this dependence is really weak (see page 480 of [29], second column).

It is interesting to notice that the nonlinear self-coherent solution (obtained with SC_{Lin1D} from equation (6), ϕ and β being unknown) in the homogeneous medium corresponds well to the Townes soliton (obtained from equation (13) with a shooting method).

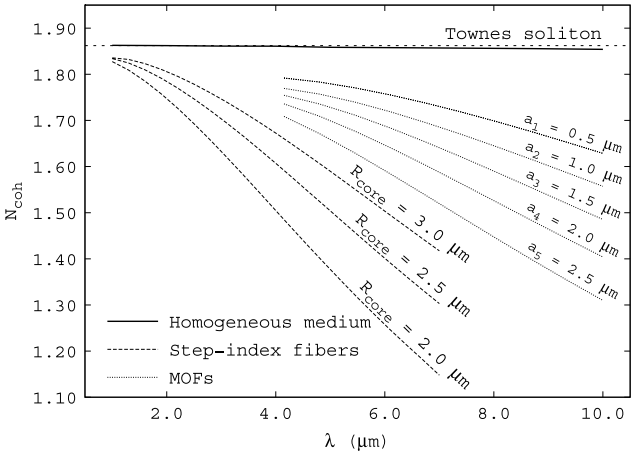

Figure 8. Evolution of the value of the self-coherent power coefficient N_{coh} for various step-index fibres, for different solid core MOFs, and for the homogeneous medium as a function of the wavelength. The horizontal dashed line is the critical power coefficient $N_{cr} = 1.862$ of the Townes soliton.

Figure 9 illustrates the dependence of the nonlinear self-coherent profile as a function of the wavelength and of the fibre geometry. The global shapes of these spatial solitons are similar that of the Townes soliton (see figure 1 in [29] and figure 1 in [30] that show clearly that the Townes soliton can be approximated with a Gaussian curve) but the amplitudes are different. As expected at a fixed wavelength, the spatial width of these spatial solitons decreases with the radius a of the air holes but the maximal amplitude increases. Nevertheless, the ratio P_{coh}/β_{coh} which appears in formula (18) decreases with a, inducing an overall decrease of the critical power coefficient N_{coh} (see also figure 8).

The next point concerns the influence of the finite size of the structure. The solid core MOF considered in figure 10 has the same geometry as that described in section 3.3 but the air hole radius is equal to 1.0 μm. The results are given for several numbers of air hole rings N_r. As can be seen in figure 10, the curve order is reversed between the linear and the nonlinear cases for the MOFs.

In the linear case and at a fixed wavelength, the effective index increases when N_r increases, which is well known [4]. In the nonlinear case, the evolution of N_r is physically coherent with the wavelength dependence already observed in figure 7: the more the structure confines the field, the lower is the nonlinear effective index. Obviously, if the air hole radius increases, the influence of the finite size structure becomes negligible. These results prove that the nonlinear self-coherent solution depends not only on the MOF structure but also on its finite size.

Last, figure 11(a) gives the evolution of the linear and nonlinear effective indices and normalized effective area versus the wavelength obtained with SC_{Lin1D} for a step-index fibre described in section 3.1.

Figure 11(a) shows that the larger the wavelength, the stronger the nonlinear effect. To confirm this observation, figure 11(b) shows that the effective area obtained in the nonlinear case is constant in comparison with the linear case.

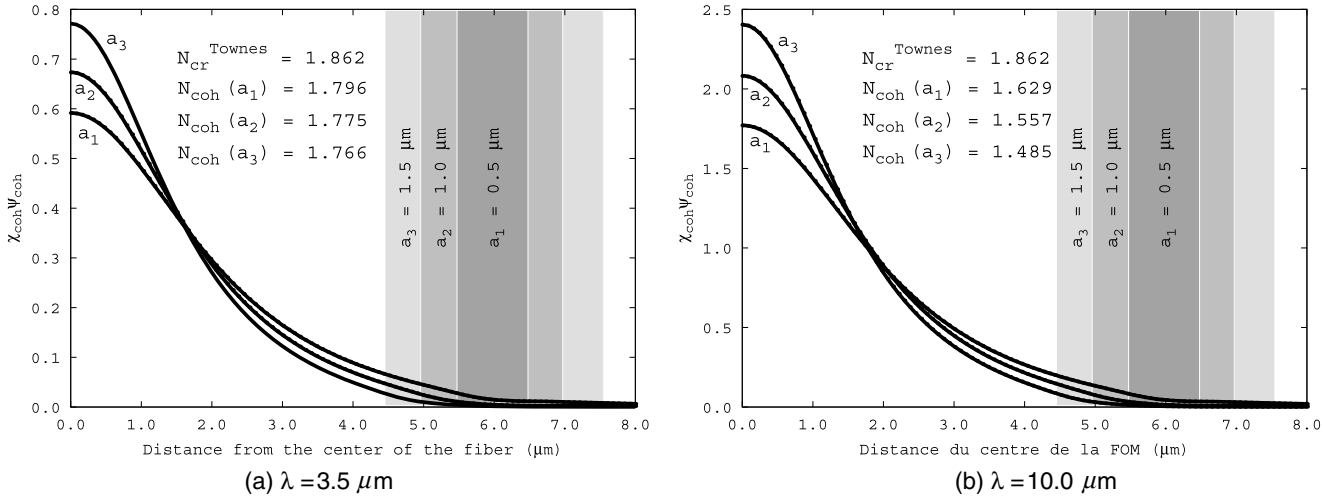

Figure 9. Field profiles for three MOFs with four air hole rings at two wavelengths. The coloured region represents the first air hole of the MOF according to the radius and the associated values of the 'self-coherent power'.

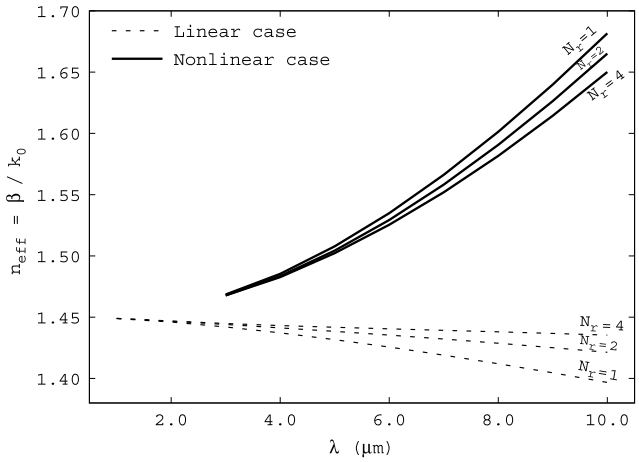

Figure 10. Effect of the number of air hole rings N_r in a solid core MOF ($\Lambda = 6.0$ μm and $a = 1.0$ μm) on the effective index according to the wavelength in the linear and nonlinear cases.

Thus, the field scattering which increases with the wavelength is challenged by the nonlinear effect.

From the results of this section, we can infer that differences from Townes soliton properties will be observed in waveguides in which the ratio of the wavelength over the characteristic size of the nonlinear core is above a constant slightly smaller that unity. Such a ratio is only three times that measured in a nonlinear glass planar waveguide [35] and can be overcome in structures like nanowires [36].

5. Discussion

The self-coherent algorithm SC_{Lin1D} has been presented for the scalar approach within the weak guidance approximation. Neglecting the term $\nabla[\mathbf{E} \cdot \nabla\epsilon_r/\epsilon_r]$, we obtain the equation $\Delta\mathbf{E} + k_0^2\epsilon_r\mathbf{E} = 0$. However, for the step-index fibre, while the weak index contrast is fulfilled in the linear case, as soon as we have considered the Kerr effect the index contrast increases and the WGA is not valid any more (see figure 12(a)). For the microstructured optical fibre, even the linear case does not obey this approximation (see figure 12(b)). Indeed, the WGA is only validated if the relative index variation is negligible on a distance of one wavelength [31]. Consequently, so as to obtain more accurate results, future studies must deal with the full vector problem. Such an extension of the present work is possible since our original numerical method can be formulated in the vector case [4, 23].

The second issue is the value of the physical power $P_{\text{phys.}} = P_{\text{coh}}/n_{\text{Kerr}}^2$ of the nonlinear self-coherent solution. This implies that the stronger the Kerr coefficient n_2 (or $n_{\text{Kerr}}^2 = 2n_0n_2$), the weaker the physical power. Nevertheless, even if we choose chalcogenide glasses which are known to have a high Kerr nonlinearity [37, 38], the power of the self-coherent solution is huge as already computed for the Townes soliton power [29]. With $n_{\text{Kerr}}^2 = 10^{-17}$ m^2 W^{-1}, one gets a soliton power of 2.6×10^4 W at 2 μm for the MOF described in section 3.3 and 7.4×10^5 W at 10 μm. These results suggest that the scalar self-coherent solution cannot easily be validated by experiments. In the scalar approach used in our study, from a practical point of view the induced increase in the refractive index of the core or of the matrix is so important that either other nonlinear effects should be taken into account or the medium is damaged [39]. However, spatial optical solitons have already been observed in planar nonlinear glass waveguides using a 4×10^5 W input at 620 nm using 75 fs pulses [35]. It will be interesting to know if, in the vector case, the physical power of the self-coherent soliton will decrease or not so as to make it more accessible to experimental observation.

The third issue of the discussion concerns the stability of the self-coherent solutions. This is a difficult problem since, in the present cases, it requires one to solve a 3D propagation problem along the waveguide axis. For the fixed-power solutions, Ferrando *et al* [17] have already proved that the spatial solitons are stable under arbitrary perturbations. They also showed that spatial solitons found at fixed power

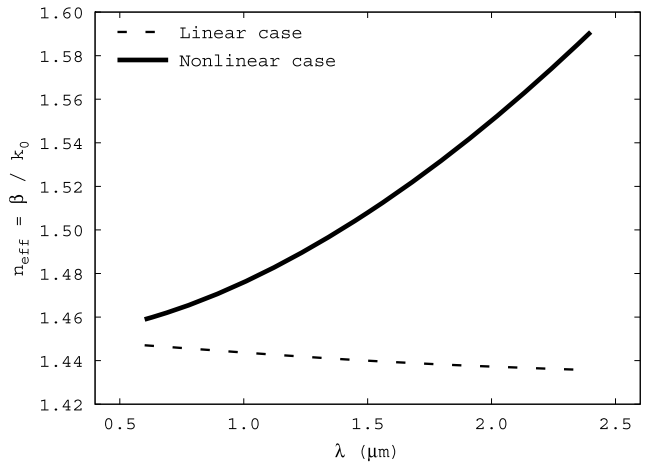

(a) Evolution of the effective indices

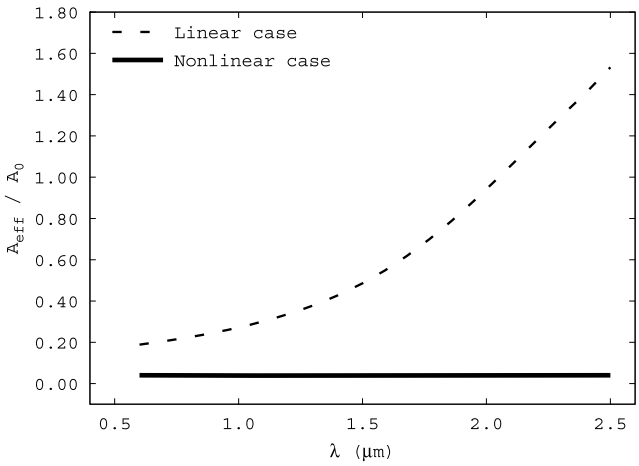

(b) Evolution of the effective area normalized with the core area $A_0 = \pi R^2_{core}$

Figure 11. Evolution of the linear and nonlinear effective indices and normalized effective area versus the wavelength for the step-index fibre described in section 3.1. For the nonlinear case, the SC_{Lin1D} algorithm is used.

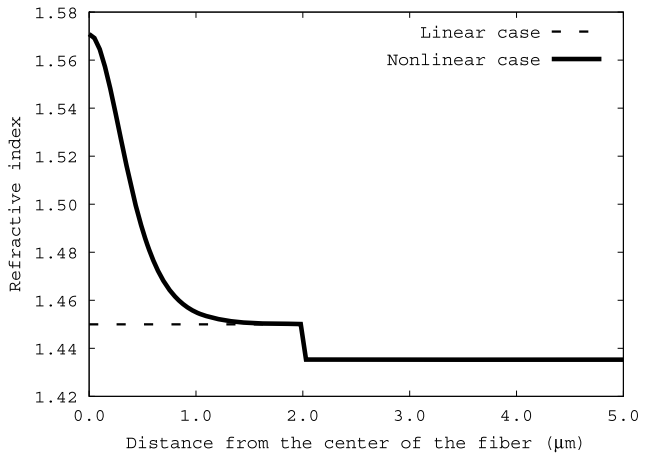

(a) Refractive index profile for the step-index fibre at λ = 1.0 μm (see section 3.1 for a complete description of the structure)

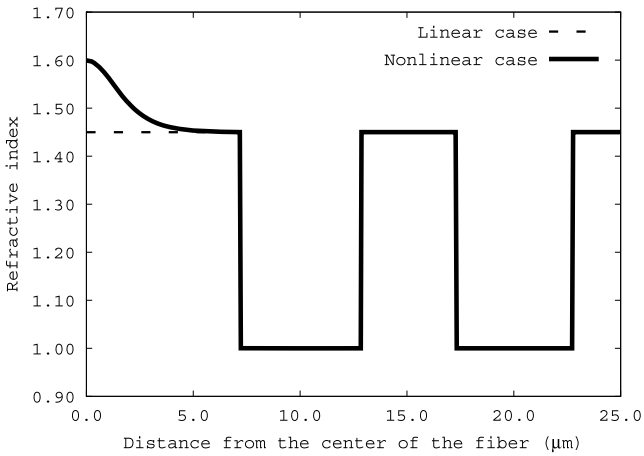

(b) Refractive index profile according to the horizontal axis of the microstructured fibre at λ = 5.0 μm (see section 3.3 for a complete description of the structure)

Figure 12. Effective index profile computed from equation (3) in the linear and nonlinear case for the fundamental 'mode' of the two fibre types described in the text.

are stable under both small transverse displacements relative to the hole cladding and non-perfect launching conditions. In the case of the self-coherent spatial solitons described in the present article, a stability analysis should also be performed. Although this issue is crucial in the case of nonlinear studies, it is beyond the scope of this initial work.

The last issue concerns the comparison with NLSE studies, as already mentioned in section 1. The counterpart of our non-paraxial description of spatial solitons is that the results we obtain are less general than the NLSE ones which can be related to both nonlinear optics and Bose–Einstein condensates [24]. Our results are not obtained with the powerful methods coming from quantum mechanics (like functional density approach) [25, 26] but with a more numerical method well adapted to our non-paraxial problem. Nevertheless, as long as stationary states are considered, our approach, which considers the nonlinear Helmholtz equation as an eigenvalue problem (with the propagation constant as an unknown), is a better model of Maxwell's equations in a nonlinear Kerr-type medium.

6. Conclusions

We have demonstrated that the nonlinear self-coherent solution found in step-index fibres and solid core MOFs, corresponding to the spatial soliton with the highest reachable energy avoiding the self-focusing instability, is different from the Townes soliton. This solution generalizes the Townes soliton within

finite size waveguides. This result, built in the frame of a non-paraxial and scalar approach for stationary solutions, relies on a new algorithm implemented using the finite element method.

To find the nonlinear self-coherent solution, two distinct criteria are defined: the convergence of the algorithm to the required accuracy (the fixed point) and the minimum of the residue at this point. By solving the eigenvalue problem, a single nonlinear solution verifying these criteria is found, for given wavelength and fibre geometry. This single solution of the eigenvalue problem is obtained with various initial guesses: the solution of the associated linear problem (SC_{Lin1D} algorithm) and some Gaussian functions ($SC_{Gauss2D}$ algorithm).

So as to verify the numerical results obtained with the self-coherent algorithm SC_{Lin1D}, several comparisons have been performed. We can adapt our numerical method to obtain a 'fixed-power' algorithm denoted FP_{FEM}. The results computed with FP_{FEM} are in good agreement with already published data for MOFs given in [17], called here FP_{Fer}. The comparison between FP_{FEM} and SC_{Lin1D} has shown that the self-coherent solution is obtained at the critical power just before the self-focusing instability. The SC_{Lin1D} algorithm is shown to be more reliable and more efficient than FP_{FEM} to find the critical power of the spatial solitons.

Then, the physical meaning of the self-coherent nonlinear solution of a step-index fibre with a Kerr material core and of solid core MOFs with Kerr material matrix is discussed. Two comparisons are made: one with the self-coherent solution computed for a homogeneous Kerr material and the second one with the usual Townes soliton computed for the same structure. From the mathematical point of view the former problem is a nonlinear eigenvalue problem while the latter is a two-point boundary value problem (since the dependence on the propagation is not taken into account.) We have shown that the self-coherent spatial solitons found for the step-index fibres and for MOFs are different from those of the homogeneous nonlinear medium and from the genuine Townes soliton. In the various structures considered in the present paper, the dependence of the self-coherent solutions is described as a function of the wavelength. We have observed that, as expected, these self-coherent spatial solitons converge towards the Townes soliton at small wavelengths. We have also observed that the amplitude of the nonlinear self-coherent solution depends on the waveguide geometry: the core size for the step-index fibre, and the air hole radius and number of air hole rings for the solid core MOFs.

Finally, the study of the refractive index induced by the nonlinear self-coherent solution has been performed. The weak guidance approximation and the scalar model are no longer valid if the self-coherent solution is considered. To tackle this problem, a study of the full-vectorial version of the proposed method, including a study of the losses, is under development.

Acknowledgments

We would like to thank Gadi Fibich and Yonatan Sivan from the Department of Applied Mathematics of Tel Aviv University for their help concerning the study of the Townes soliton profile.

References

[1] Kuhlmey B, White T P, Renversez G, Maystre D, Botten L C, de Sterke C M and McPhedran R C 2002 Multipole method for microstructured optical fibers II: implementation and results *J. Opt. Soc. Am.* B **10** 2331–40

[2] Kuhlmey B, Renversez G and Maystre D 2003 Chromatic dispersion and losses of microstructured optical fibers *Appl. Opt.* **42** 634–9

[3] Renversez G, Bordas F and Kuhlmey B T 2005 Second mode transition in microstructured optical fibers: determination of the critical geometrical parameter and study of the matrix refractive index and effects of cladding size *Opt. Lett.* **30** 1264–6

[4] Zolla F, Renversez G, Nicolet A, Kuhlmey B, Guenneau S and Felbacq D 2005 *Foundations of Photonic Crystal Fibres* (London: Imperial College Press)

[5] Agrawal G P 2001 *Nonlinear Fiber Optics* 3rd edn (New York: Academic)

[6] Kivshar Y S and Agrawal G P 2003 *Optical Solitons* (Amsterdam: Academic)

[7] Chen Y and Atai J 1997 Maxwell's equations and the vector nonlinear Schrödinger equation *Phys. Rev.* E **55** 3652–7

[8] Akhmediev N, Ankiewicz A and Soto-Crespo J M 1993 Does the nonlinear Schrödinger equation correctly describe beam propagation? *Opt. Lett.* **18** 411

[9] Ciattoni A, Crossignani B, Di Porto P and Yariv A 2005 Perfect optical solitons: spatial Kerr solitons as exact solutions of Maxwell's equations *J. Opt. Soc. Am.* B **22** 1384–94

[10] Karlsson M, Anderson D, Desaix M and Lisak M 1991 Dynamic effects of Kerr nonlinearity and spatial diffraction on self-phase modulation of optical pulses *Opt. Lett.* **16** 1373

[11] Karlsson M, Anderson D and Desaix M 1992 Dynamics of self-focusing and self-phase modulation in a parabolic index optical fiber *Opt. Lett.* **17** 22

[12] Ciattoni A, Crossignani B, Di Porto P, Scheuer J and Yariv A 2006 On the limit of validity of nonparaxial propagation equations in Kerr media *Opt. Express* **14** 5517–23

[13] Selleri S, Vincenti L and Cucinotta A 1998 Finite element method resolution of non-linear Helmholtz equation *Opt. Quantum Electron.* **30** 457–65

[14] Joseph R M and Taflove A 1994 Spatial soliton deflection mechanism indicated by FD-TD Maxwell's equations modeling *IEEE Photon. Technol. Lett.* **6** 1251–4

[15] Feit M D and Fleck J A Jr 1988 Beam nonparaxiality, filament formation, and beam breakup in the self-focusing of optical beams *J. Opt. Soc. Am.* B **5** 633

[16] Nicolet A, Drouart F, Renversez G and Geuzaine C 2007 A finite element analysis of spatial solitons in optical fibres *COMPEL* **26** 1105–13

[17] Ferrando A, Zacarés M, Fernandez de Cordoba P, Binosi D and Monsoriu J A 2003 Spatial soliton formation in photonic crystal fibers *Opt. Express* **11** 452–9

[18] Ferrando A, Zacares M, Fernandez de Cordoba P and Monsoriu J A 2004 Vortex solitons in photonic crystal fibers *Opt. Lett.* **12** 817–22

[19] Snyder A W, Mitchell D J and Chen Y 1994 Spatial solitons of Maxwell's equations *Opt. Lett.* **19** 524–6

[20] Snyder A W, Hewlett S J and Mitchel D J 1994 Dynamic spatial solitons *Phys. Rev. Lett.* **72** 1012–5

[21] Nicolet A, Guenneau S and Zolla F 2004 Modelling of twisted optical waveguides with edge elements *Eur. Phys. J. Appl. Phys.* **28** 153–7

[22] Boyer P, Renversez G, Popov E and Nevière M 2007 Improved differential method for microstructured optical fibres *J. Opt. A: Pure Appl. Opt.* **9** 728–40

[23] Guenneau S, Nicolet A, Zolla F and Lasquellec S 2002 Modeling of photonic crystal fibers with finite elements *IEEE Trans. Magn.* **38** 1261–4
[24] Alexander T J and Bergé L 2002 Ground states and vortices of matter–wave condensates and optical guided waves *Phys. Rev.* E **65** 026611
[25] Dalfovo F, Renversez G and Treiner J 1992 Vortices with more than one quantum of circulation in He-4 at negative-pressure *J. Low Temp. Phys.* **89** 425–8
[26] Dalfovo F, Giorgini S, Pitaevskii L P and Stringari S 1999 Theory of Bose–Einstein condensation in trapped gases *Rev. Mod. Phys.* **71** 463–512
[27] García-Ripoll J J and Pérez-García V M 2001 Optimizing Schrödinger functionals using Sobolev gradients: applications to quantum mechanics and nonlinear optics *SIAM J. Sci. Comput.* **23** 1315–33
[28] Ablowitz M J, Ilan B, Schonbrun E and Piestun R 2006 Solitons in two-dimensional lattices possessing defects, dislocations, and quasicrystal structures *Phys. Rev.* E **74** 035601
[29] Chiao R Y, Garmire E and Townes C H 1964 Self-trapping of optical beams *Phys. Rev. Lett.* **13** 479–82
[30] Fibich G and Gaeta A L 2000 Critical power for self-focusing in bulk media and in hollow waveguides *Opt. Lett.* **25** 335–7
[31] Marcuse D 1991 *Theory of Dielectric Optical Waveguides* 2nd edn (San Diego, CA: Academic)
[32] Snyder A W and Love J D 1983 *Optical Waveguide Theory* (New York: Chapman and Hall)
[33] Boyd R W 2003 *Nonlinear Optics* 2 edn (New York: Academic)
[34] Press W H, Flannery B P, Teukolsky S A and Vetterling W T 1986 *Numerical Recipes* (Cambridge: Cambridge University Press)
[35] Aitchison J S, Weiner A M, Silberberg Y, Oliver M K, Jackel J L, Leaird D E, Vogel E M and Smith P W E 1990 Observation of spatial optical solitons in a nonlinear glass waveguide *Opt. Lett.* **15** 471–3
[36] El-Ganainy R, Mokhov S, Makris K G, Christodoulides D N and Morandotti R 2006 Solitons in dispersion-inverted AlGaAs nanowires *Opt. Express* **14** 2277–82
[37] Smektala F, Quemard C, Couderc V and Barthélémy A 2000 Non-linear optical properties of chalcogenide glasses measured by *z*-scan *J. Non-Cryst. Solids* **274** 232–7
[38] Brilland L, Smektala F, Renversez G, Chartier T, Troles J, Nguyen T, Traynor N and Monteville A 2006 Fabrication of complex structures of holey fibers in chalcogenide glass *Opt. Express* **14** 1280–5
[39] Stuart B C, Feit M D, Rubenchik A M, Shore B W and Perry M D 1995 Laser-induced damage in dielectrics with nanosecond to subpicosecond pulses *Phys. Rev. Lett.* **12** 2248–51